

# Development of Self-folded Corrugated Structures Using Automatic Origami Technique by Inkjet Printing

Yuki Fukatsu<sup>1</sup> and Hiroki Shigemune<sup>1</sup>

<sup>1</sup>Affiliation not available

April 5, 2022

## Abstract

The origami technique realizes unique mechanical properties of sheet materials without additional parts. In this study, a self-folded corrugated structure (SCS) is developed based on the reinforcing properties of the origami technique. The corrugated structures are employed as the core material for a high-strength, open-channel sandwich structure. Research on self-folded core materials is scarce; thus, a design concept is proposed, and the mechanical properties of the SCS are evaluated. First, the structural parameters of the SCS fabricated by changing the printing parameters (e.g., linewidth and number of lines/creases), to derive the structural model are determined. The model facilitates the design of an SCS with the desired structure. Thereafter, the mechanical properties of the SCSs are evaluated by conducting three-point bending tests to determine the essential design parameters corresponding to high stiffness. Moreover, SCSs can be stacked without occupying space, thus leading to improved strength. These SCSs fabricated using self-folding paper by ink-jet printing are low cost and eco-friendly. Moreover, they are specialized for rapid design and fabrication, depending on the application. This paper proposes the use of SCS as a novel smart core because it exhibits a high transportation efficiency and stiffness without additional components.

Corresponding author(s) Email: ae18081@shibaura-it.ac.jp , hshige@shibaura-it.ac.jp

## ToC Figure

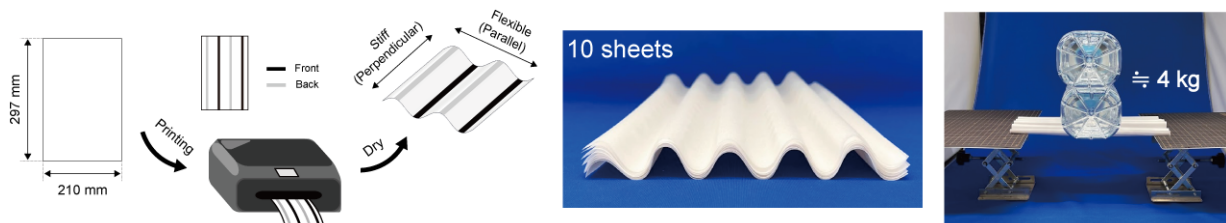


Figure 1: **ToC Figure.** A corrugated structure is created by the self-folding of a smart material. Strength is freely designable according to the printing pattern, and the flexibility of the structure allows for stacking to improve strength. The stacked structure can withstand a load of about 4 kg. A promising new smart core made by inkjet printing is proposed in this paper.

## Introduction

Origami is a technique for creating complex three-dimensional (3D) structures by defining mountain and valley crease patterns on a two-dimensional (2D) sheet. The defined crease patterns impart various properties to the formed 3D structures. One of the properties imparted is foldability and expandability to compactly store the deployable structures. These properties allow for the fabricated 3D structure to be folded into a 2D shape and redeployed at the destination. These properties have led to applications in medical stents [1], automotive airbags [2], shelters [3], and space structures [4]. In addition, the crease patterns have properties that increase the structural strength of 3D structures. Specifically, the crease patterns increase the stiffness of the entire structure by increasing the second area moment. The stiffness can be increased by three orders of magnitude by adding straight creases while using the same amount of material [5] [6]. In addition, the microstructure folded with lithographic patterning can withstand a load greater than its weight by a factor of 7700 [7]. Therefore, this technique has been used to manufacture core materials for sandwich structures, as they are lightweight and exhibit high stiffness.

The sandwich structure consists of two-face sheets sandwiching the core material. A honeycomb core is widely used as one of the core materials [8]. However, the manufacture of honeycomb cores is complex and costly. Therefore, extensive research has been conducted on honeycomb cores based on the origami technique [9]. In this regard, the origami technique enables the manufacturing of honeycomb cores without considerable processing. Folded cores based on origami are currently developed as alternative core materials. Examples include Miura-ori, which is commonly used to shape folded cores [10], and creases similar to Ron Resch patterns [11]. Folded cores can be manufactured from various sheet materials by a simple process and tailored into various shapes that meet specific functional requirements [12]. Thus, the origami technique has been applied to core materials for sandwich structures.

On the contrary, corrugated cores are stiff, perpendicular to the corrugation, flexible in the parallel direction, and the structures exhibit anisotropy [13]. This property is leveraged in load-bearing applications such as corrugated cardboards, roofs, and walls, in addition to morphing wings [14]. In contrast, the folded core is stiff in the perpendicular and parallel directions. The stiff direction of a corrugated core with linear creases is stiffer than that of the folded core by a factor greater than 75 [5] [6]. The closed-cell structures lead to problems of air and humidity retention, which can increase the total weight and degrade core properties [15]. Conversely, corrugated cores have open channels in one direction, which minimizes these problems.

Corrugated, honeycomb, and folded cores can be readily fabricated using the origami technique. Origami structures can be fabricated by manual folding or by using robotic devices [16]. However, these methods are not efficient for mass production at small or large scales and for remote applications. Mass production can be realized using manufacturing equipment; however, large machines require space allocation and initial investment, and the compression process consumes large amounts of energy. Moreover, it compromises the specialized feature of creating structures with desired mechanical properties within a short time.

To overcome these shortcomings, self-folding techniques have been studied for the automatic fabrication of origami structures [17]. Self-folding generally uses smart materials that respond to external stimuli, such as shape memory alloy (SMA) [18], shape memory polymer (SMP) [19], and hydrogel [20]. The crease pattern is pre-defined for these smart materials, and the application of heat or light triggers automatic folding. Given that external stimuli automatically form the origami structure, rapid manufacture and autonomous assembly at remote sites can be achieved without human intervention. Moreover, given that 3D structures can be constructed by changing the 2D crease patterns, a variety of origami structures can be created. Liu et al. proposed self-folding SMP sheets using light. They defined crease patterns to fold SMP sheets by 90° and fabricated a rectangular shape. By changing the crease patterns, the fold angle was adjusted to 60°, and a tetrahedron structure was formed [21].

Besides the origami technique, core materials for sandwich structures are manufactured by compression molding [22], hot-press molding [23], and embossing with rollers, among other methods [24]. However, these manufacturing methods require molds and rollers for each design requirement, which increases the

cost, time, and energy required to form the structure. Therefore, core materials fabricated with 3D printing technology, which can be used to design complex structures at low cost, have been developed [25][26][27]. Furthermore, the development of core sandwich structures using smart active materials, which are referred to as smart cores, was investigated [28]. Tolley et al. fabricated a self-folding origami consisting of a three-layer shape memory composite with SMP as the intermediate layer to form a Miura-ori structure [29]. Evans et al. fabricated a micro-scale self-folding origami structure consisting of three layers of photo-cross-linkable copolymers with a thermosensitive hydrogel as the intermediate layer. They realized a Miura-ori structure by controlling the fold angle [30]. However, limited studies were conducted on the mechanical properties of the smart core sandwich structures. Hubbard et al. fabricated corrugated structures with rectangular, square, trapezoidal, and triangular waveforms using stimuli-responsive thermoplastic sheets [31]. They conducted compression and tensile tests by varying the wavenumbers of the fabricated corrugated structures, and investigated the effects of the wavenumbers on the compressive and tensile properties of the structures. However, mechanical properties were not investigated with respect to the amplitude and wavelength, which are important structural parameters of the corrugated structure when using the tailor-made feature of the self-folding methods. By investigating the mechanical properties with respect to the amplitude and wavelength, the desired mechanical properties can be imparted to the structure and specialized characteristics can be realized. Therefore, we conducted experiments to investigate the mechanical properties of corrugated structures with respect to the amplitude and half-wavelength, which are the two most important structural parameters of the corrugated structure.

In this study, we developed a corrugated structure made of a smart material. A design theory of the structure was proposed, and its mechanical properties were evaluated. We denote the developed structure as a self-folded corrugated structure (SCS). Based on the reaction between a smart material and inkjet printer ink, the structure was formed autonomously without applying external energy. First, we proposed a structural model to predict the final shape of the SCS from the printed pattern. By calculating the fold angle from the proposed model, a linear relationship between the printed linewidth and the fold angle was obtained, similar to the conventional method [32], which validated the proposed model. The design parameters of the SCS were the printed line width and number of printed lines. Self-folded corrugated structures with various amplitudes and wavelengths were formed by varying the parameters. Second, the mechanical properties of the SCS were evaluated by conducting a three-point bending test. The results revealed that the SCS exhibited anisotropic stiffness, which is one of the typical properties of corrugated structures. In addition, with an increase in the amplitude of the SCS, the second area moment increased, as expressed by the theoretical equation of the second area moment of corrugated structures. As a characteristic of the SCS, we confirmed that, for a large wavelength range, the structure collapses due to the flexibility of the paper. Furthermore, we found that the SCS is sufficiently flexible for easy stacking after self-folding. The structural strength of the SCS can be improved linearly by stacking structures. Thus, the fabrication system of the SCS provided stiffness to a sheet of paper, which is innately flexible to be applied as a core material. Given that the only fabrication method is the application of solution by inkjet printing, the corrugated structure with the desired stiffness can be created rapidly according to the desired applications. Moreover, the SCS can be stacked without occupying a significant amount of space, thus minimizing energy consumption during transportation and reducing the transportation costs. Therefore, the SCS will be developed as a novel smart core for future applications owing to its high stiffness, digital manufacturing ability, and high transportability.

## Concept of the Self-Folded Corrugated Structure

**Figure 2a** presents the fabrication process of the SCS using inkjet printing. In this experiment, A4 size paper (210 mm × 297 mm) with a thickness of 80.5 μm (XDT Tracing FS, TAKEO Co.) was used. The materials used were introduced in previous studies [32] [33] [34]. By inkjet printing on the A4 paper, which is then set aside, valley folds are automatically formed along the printing lines. The self-folding process of paper is as follows. The reaction between paper and ink causes the fibers to expand and contract. During

the expansion phase, the top surface of the paper expands, causing the paper to fold into a mountain fold against the printing surface. This is followed by a contraction phase, in which the paper folds into valley folds against the printing surface. As plastic deformation occurs, the origami structure is fixed in the valley-folded state [32]. Figure 2b and c present the process of SCS formation during the contraction phase. To form mountain and valley folds, a printing pattern is defined on both sides. In this study, we fabricated an SCS by inkjet printing under humidity levels ranging from 55% to 65% ( $\pm 3\%$  RH), and set it aside for approximately 10 min. As the paper transformed into an SCS, it developed stiffness anisotropy; thus, it increased in stiffness in the direction perpendicular to the corrugation, and in flexibility in the parallel direction. The fabricated SCS was placed in a sealed container with a desiccant and stored in a low-humidity environment.

Figure 2b presents the self-folding process of the SCS with four creases. Immediately after printing (Figure 2b(i)), mountain folds are formed on the prior-printed side. Given that both sides cannot be printed simultaneously, there is a time lag between the folding times of the mountain folds and the valley folds due to the time required to set the printer. After 60 s (Figure 2b(ii)), the side printed subsequently starts to fold. After 600 s (Figure 2b(iii)), folding on both sides is completed, and the SCS is formed with the mountain and valley folds (**Figure 3**). Figure 2c presents the self-folding process of the SCS with the number of creases increased to 10 (**Figure 4**).

Figure 2d presents a demonstration, wherein the paper is transformed into an SCS with increased stiffness. The central part of the structure is fixed to a wooden board with double-sided tape. As shown on the left side of the figure, the sheet of paper without the SCS cannot withstand its self-weight and bends downward. Conversely, as shown on the right, the SCS structure can support its own weight without deflection. The SCS improves the second area moment and stiffness of the paper. Furthermore, a number of SCS sheets can be stacked to increase the stiffness without occupying significant space. Figure 2e presents a demonstration of the stacked SCS, wherein an SCS stacked with 10 sheets withstands a mass of approximately 4 kg (**Figure 5**).

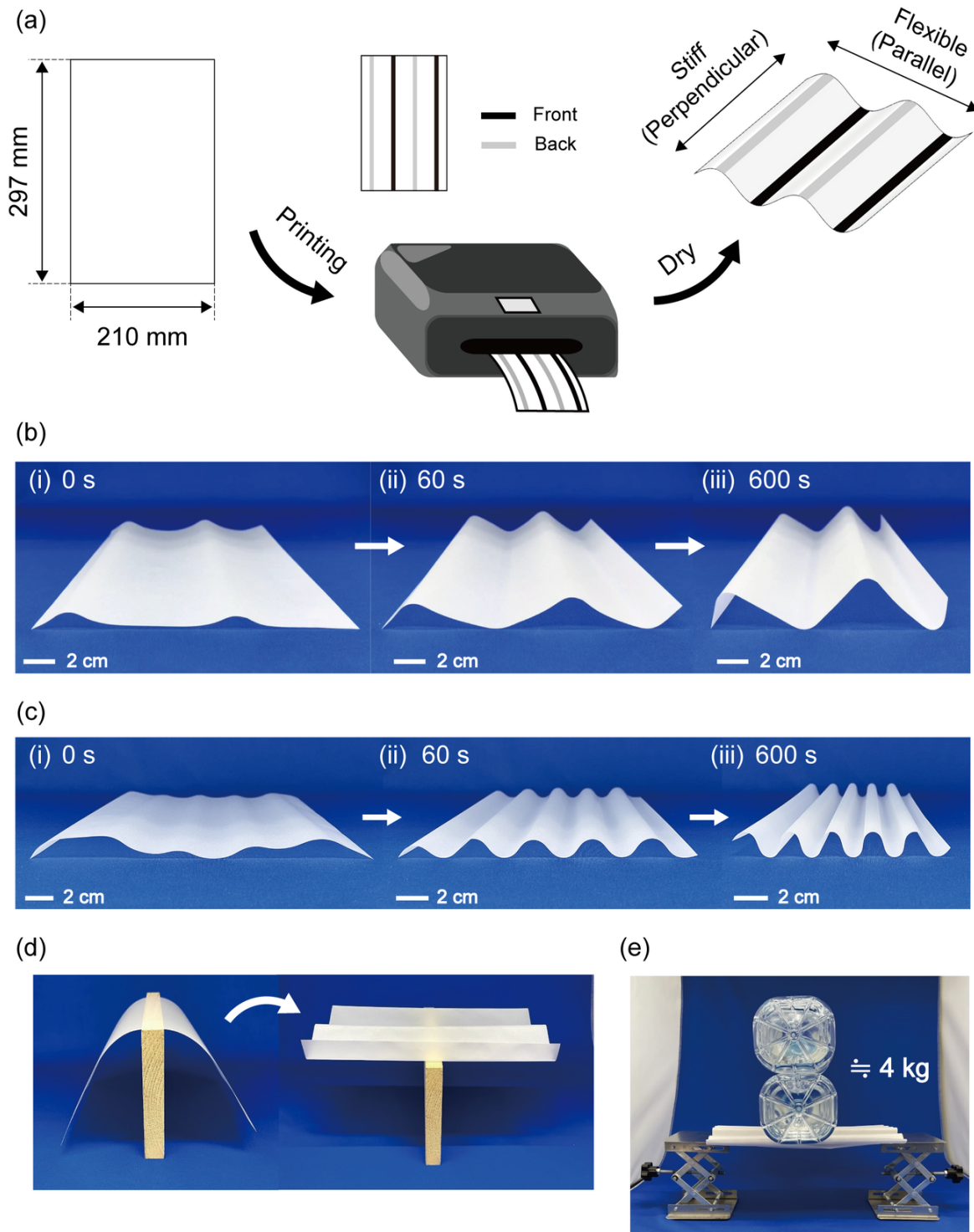


Figure 2: Self-folded corrugated structure (SCS). (a) Conceptual diagram of the SCS fabrication process. The SCS is fabricated by defining the printing pattern on both sides and inkjet printing. (b) Self-folding process of the SCS with four creases and (c) 10 creases. The SCS required 600 s to self-fold after printing. (d) Demonstration of the SCS. A single sheet of paper deflects under its self-weight; however, the SCS can support its self-weight by increasing the second area moment. (e) Demonstration of stacking the SCS. A stack of 10 sheets can withstand a mass of about 4 kg.

Rich media available at <https://youtu.be/khWODtu-12c>

Rich media available at <https://youtu.be/0wW2qcU-YH4>

Rich media available at <https://youtu.be/3kQbWAerjHk>

## Design of Self-Folded Corrugated Structure

### Effect of Design Parameters

This section discusses the design method of the SCS based on the self-folding of paper. As shown in **Figure 6a(i)**, the linewidth  $L$  and number of lines  $n$  are defined as the design parameters. These two design parameters determine a line interval  $i$ . With the design shown in Figure 6a(i), the cross-sectional corrugation is formed in the horizontal direction (length of 210 mm) of the paper. Thus,  $i$  is expressed by the following equation:

$$i = \frac{210}{n} - L \quad (1)$$

By design, as shown in Figure 6a(i), a cross-sectional corrugation with amplitude  $d$  and half-wavelength  $w$  is formed at each crease, as shown in Figure 6a(ii). Moreover,  $L$  can then be considered as an arc of the cross-sectional corrugation; and  $n$  changes the number of creases, thus resulting in a change in the number of half-wavelengths in the cross-sectional corrugation. In the experiment, we ensured that  $n$  was equal to the number of half wavelengths by setting the line interval as  $i/2$  between both edges. The remainder of this sub-section discusses the effects of the design parameters,  $L$  and  $n$ , on the final shape of the SCS.

First, we investigated the effect of  $L$  on the shape of the SCS. Figure 6b presents an example of an SCS designed with  $n = 4$  and  $L = 5$  mm, 10 mm, and 15 mm. As can be seen from the figure, with an increase in the linewidth, the paper folded more, i.e., the arc length increased, assuming that the curvature was constant for any linewidth. Consequently, the gradient of the straight-line parts joining each arc increased. Therefore, as  $L$  increased, the amplitude of the corrugated structure  $d$  increased, and the half-wavelength  $w$  decreased. Thus,  $d$  and  $w$  were found to be inversely proportional.

Thereafter, we investigated the effect of  $n$  on the shape of the SCS. Figure 6c presents an example of the SCS with  $L = 15$  mm and  $n = 4, 6, 8,$  and  $10$ . As shown in Figure 6c, the number of  $w$  corresponds to  $n$ . In this study, all SCSs were fabricated in A4 size. With an increase in the number of half-wavelengths, the length of paper required to form one half-wavelength decreased. Therefore, as  $n$  increased,  $d$  and  $w$  decreased. The length of the paper required to form one half-wavelength  $w_{\max}$  is determined by the following equation:

$$w_{\max} = \frac{210}{n} \quad (2)$$

The effects of the linewidth  $L$  and the number of lines  $n$  on the amplitude  $d$  and half-wavelength  $w$  of the cross-sectional corrugation were verified based on measured values. In an experiment, 60 SCSs were fabricated by changing  $L$  by 1 mm in the range of 1–15 mm for each structure with  $n = 4, 6, 8,$  and  $10$ . Thereafter, the amplitude  $d$  and the half-wavelength  $w$  of the cross-sectional corrugation were measured. Figure 6d presents

the results of the experiment, with the amplitude  $d$  as a circle plot and the half-wavelength  $w$  as a cross plot. To improve legibility, the horizontal axis was set as  $i$ , which is determined by  $L$  and  $n$  from Equation (1). From the blue plot ( $n = 4$ ), as  $i$  decreased,  $L$  increased. Subsequently,  $d$  increased, and  $w$  decreased. The trend was the same for all the structures with  $n = 6, 8, \text{ or } 10$ . Additionally, as  $n$  increased, the changes in the amplitude and half-wavelength with respect to the linewidth decreased due to the decrease in the length of paper required to form one half-wavelength  $w_{\max}$ .

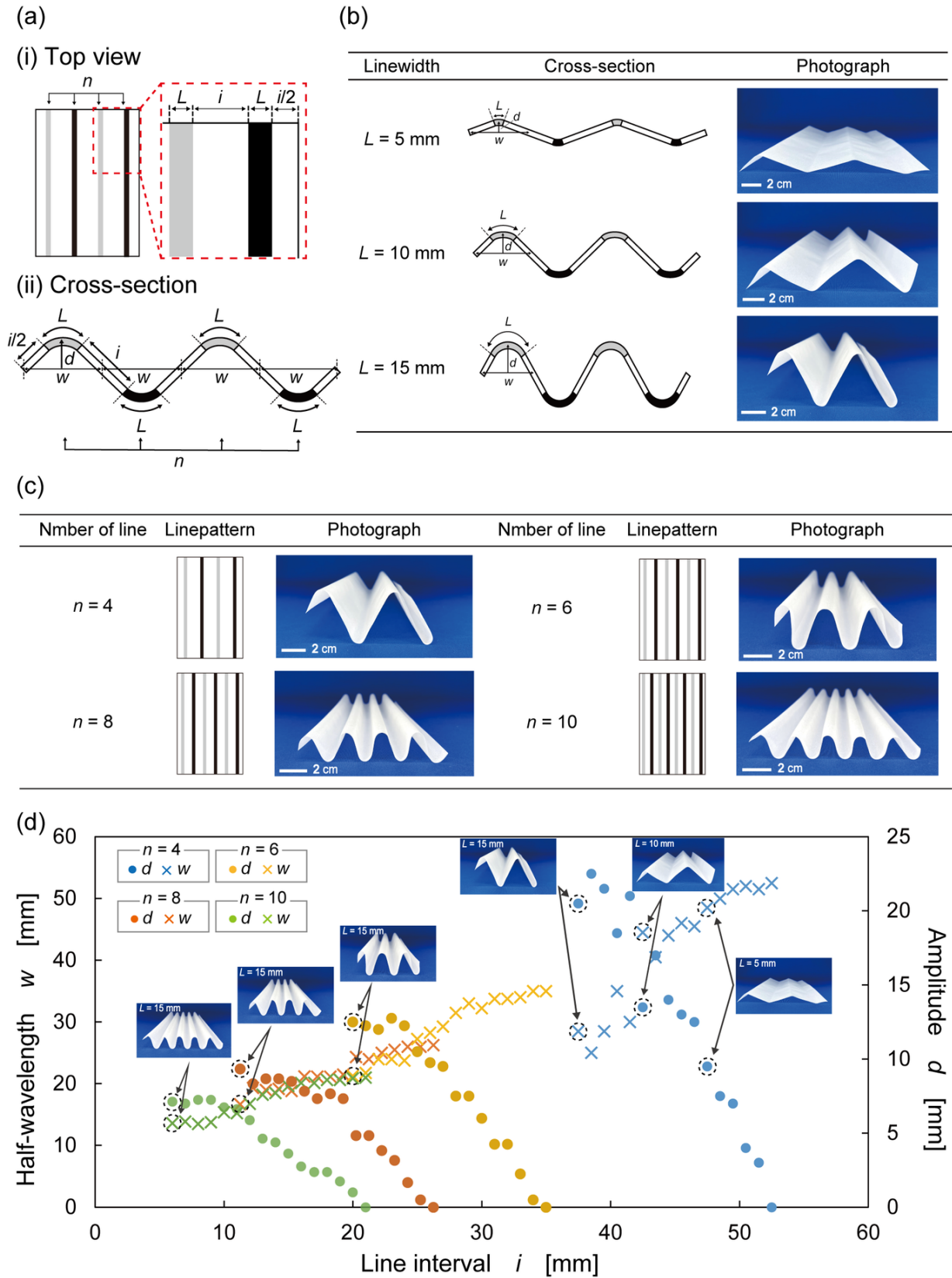


Figure 3: Design concept of the SCS. a) Definition of (i) design parameters and their correspondence to (ii) structural parameters. b) Effect of linewidth  $L$  on the SCS formation. As  $L$  increased, the amplitude  $d$  of the SCS increased, and the half-wavelength  $w$  decreased. c) Effect of  $n$  on the SCS formation, where  $n$  corresponds to the number of half-wavelengths. d) Relationship between the line interval  $i$  and  $d$  and  $w$ , as determined using 60 samples of the SCS. The circle plots represent the amplitude, and the cross plots represent the half-wavelength.

## Modeling

As shown in **Figure 7**, the SCS was modeled based on the design concept. The cross-sectional corrugations were modeled by approximation as triangles, as shown in Figure 7a. Thereby, the SCS formation angle  $2\alpha$  and fold angle  $\theta$  are defined as follows:

$$2\alpha = 2 \tan^{-1} \frac{w}{2d} \quad [] \quad (3)$$

$$\theta = 180 - 2\alpha \quad [] \quad (4)$$

We substituted the measured values of the amplitude  $d$  and the half-wavelength  $w$ , as obtained from Figure 6d, into Equation (3), and then calculated the SCS formation angle  $2\alpha$ . The fold angle  $\theta$  was calculated from Equation (4). Figure 7b presents the relationship between  $\theta$  and  $L$ . Based on a linear approximation of the plot in Figure 7b,  $\theta$  and  $L$  are defined from the fold coefficient  $m$  by the following equation:

$$j = mL \quad [] \quad (5)$$

This linear relationship between the linewidth and fold angle was confirmed in previous research [32]. Figure 7c reveals that the coefficient of determination  $R^2$  values were close to 1 for all numbers of lines; thus, the triangle approximation can be considered appropriate. Although, for the same linewidth,  $\theta$  differs according to  $n$ . The value of  $m$  decreases as  $n$  increases. This is due to the difference between the “folding” and “bending” of the SCS creases, as discussed by Liu et al [35]. When the linewidth is low ( $L = 5$  mm), as shown in Figure 7d, the error of the triangle approximation is small because the creases are far from each other. When the linewidth is low ( $L = 5$  mm), as shown in Figure 7d, the creases are closer to the “folding” shape, and the error of the triangle approximation is smaller because the creases are far from each other. However, as the linewidth increases ( $L = 15$  mm) and shifts to a “bending” shape, the effect of the approximation increases, and  $\theta$  decreases. As shown in Figure 7e, the more the number of lines, the closer the folds, and the shorter the straight-line parts. Therefore, with an increase in the number of lines, the creases shift toward a “bending” shape as the linewidth changes. Consequently, if the distance between the lines is small, the change in the gradient of the straight-line parts caused by the linewidth is difficult to observe, and the observed value is smaller than the actual value. Thereafter, we derived the relationships between  $L$  and  $d$  and  $L$  and  $w$  from the fold angle. The diagonal side  $i/2 + L/2$  of the right triangle shown in Figure 7a is defined from Equation (1) as follows:

$$\frac{i}{2} + \frac{L}{2} = \frac{105}{n} \quad (6)$$

Therefore, the amplitude  $d$  and half-wavelength  $w$  are obtained from Equation (4) and (5).

$$d = \frac{105 \cos \alpha}{n} = \frac{105 \cos[?](90 - \frac{mL}{2})}{n} \quad (7)$$

$$w = \frac{210 \sin \alpha}{n} = \frac{210 \sin(90 - \frac{mL}{2})}{n} \quad (8)$$

The measured values of  $d$  and  $w$  were plotted as shown in Figure 7f and g, where Equation (7) and (8) are represented as solid lines. The fold coefficient  $m$  required for the theoretical equation is the value derived in Figure 7c. As shown in Figure 7f and g, the measured values and the theoretical equations are in good agreement. The parameters  $d$  and  $w$  can be derived from the design parameters  $L$  and  $n$ . Using this model, we can design the printing pattern for the structural parameters of the desired SCS ( $d$  and  $w$ ). This model equation can be applied to structures with other values of  $n$ , and SCSs with the desired number of half-wavelengths can be designed based on the application.

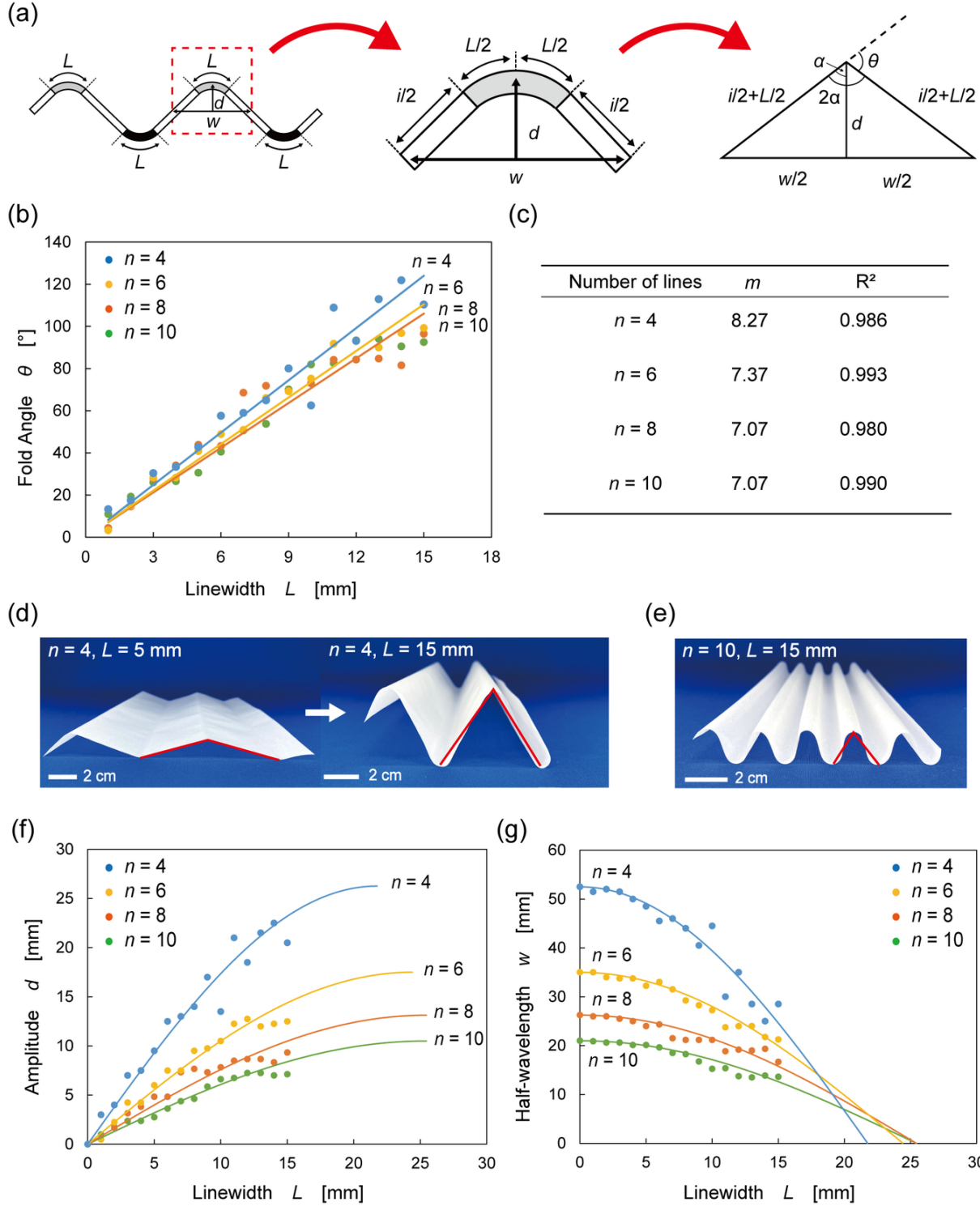


Figure 4: Modeling of the SCS. a) Triangle approximation of the corrugation. b) The relationship between the linewidth  $L$  and fold angle  $\vartheta$ . c) The fold coefficient  $m$  and the coefficient of determination  $R^2$ , as calculated from the linear approximation. d, e) Verification of the triangle approximation. The transition of f) amplitude  $d$  and g) half-wavelength  $w$  with respect to  $L$ . The measured values and proposed model equation are in good agreement.

# Evaluation of SCS

## Evaluation Method

We evaluated the stiffness of the SCS by conducting a three-point bending test. **Figure 8a** presents a schematic of the test. We used a tension and compression testing machine (Shimadzu, AG-50kNX) to conduct the test for both ends supported with a concentrated load. The test conditions were as follows: the displacement speed was set at 5.00 mm/min, the load was applied until the stroke reached 30 mm, and the data were recorded with a sampling period of one point per second. Twelve types of SCSs with  $n = 4, 6, 8,$  and  $10$  and  $L = 5$  mm,  $10$  mm, and  $15$  mm were tested. A load bar was attached to the testing machine, such that the load could be applied only to the center of the SCS (**Figure 8a(i)**). A wooden board was placed, such that the distance between fulcrums was 280 mm, and the SCS was fixed by pins inserted into the valley folds (**Figure 8a(ii)**). **Figure 8a(iii)** presents a photograph of the actual test. The valley fold was not formed at one end of the SCS (**Figure 8a(iv)**). **Figure 9** presents a movie of the actual test.

**Figure 8a(v)** presents the beams in a three-point bending test of both ends supported with a concentrated load. The relationship between the load  $P$  and deflection  $\delta$  is expressed as the following equation:

$$\delta = \frac{Pl^3}{48EI} \quad (9)$$

Where  $l$  is the distance between the fulcrums,  $E$  is Young's modulus, and  $I$  is the second area moment, which can be obtained from Equation (9).

$$I = \frac{Pl^3}{48\delta E} \quad (10)$$

Using  $I$ , the stiffness of the SCS can be evaluated. The distance between the fulcrums  $l$  was 280 mm, and Young's modulus of the paper  $E$  derived from the tensile test was 5.32 GPa (**Figure S1**). We fabricated three of each 12 types of SCSs as samples and conducted a total of 36 tests. The three test results obtained for each structure were averaged.

**Figure 8b** presents a sample result of a load-deflection curve obtained from a three-point bending test. In this section, an area of up to 10 mm of the entire 30 mm stroke was excerpted to better understand the analysis method. To derive the second area moment from the load-deflection curve, an explanation of the three stages (i)–(iii) shown in **Figure 8b** is presented. The load bar descends in the first stage; however, it is not in contact with the SCS (**Figure 8b(i)**). Then, as the load bar continues to descend, it contacts the SCS (**Figure 8b(ii)**). This point is regarded as the starting point of the three-point bending test, and is the origin of the load-deflection curve. In this study, the starting point was located within the stroke range of 0–5 mm for all structures tested; however, there was variation among the structures. Therefore, the test was conducted up to a stroke of 30 mm, and the deflection  $\delta$  was unified in the range of 0–25 mm in the load-deflection curve. In the final stage, the mountain fold parts collapsed as the load was applied to the SCS until its peak was reached (**Figure 8b(iii)**). The stiffness  $k$  can be calculated from the slope of the initial stage in the range from the test start point to the peak. In this experiment, the increase in the deflection  $\delta$  from 0 mm to 2 mm was defined as the slope of the initial stage.

$$I = \frac{Pl^3}{48\delta E} = \frac{kl^3}{48E} \quad (11)$$

We confirmed the presence of stiffness anisotropy, which is one of the typical properties of the corrugated structure, by conducting a three-point bending test in two directions ( $x$  and  $y$ ), as shown in **Figure 8c**. Given that the tension and compression testing machine (Shimadzu, AG-50kNX) did not allow the installation of wooden plates in the  $y$ -direction, we used a desktop type tension and compression testing

machine (A&D, MCT-1150) for the  $y$ -direction compression. Figure 8d presents the load-deflection curves obtained from the three-point bending tests conducted in both directions. The results reveal that the stiffness was high in the  $x$ -direction and low in the  $y$ -direction, which is a typical property of the corrugated structure.

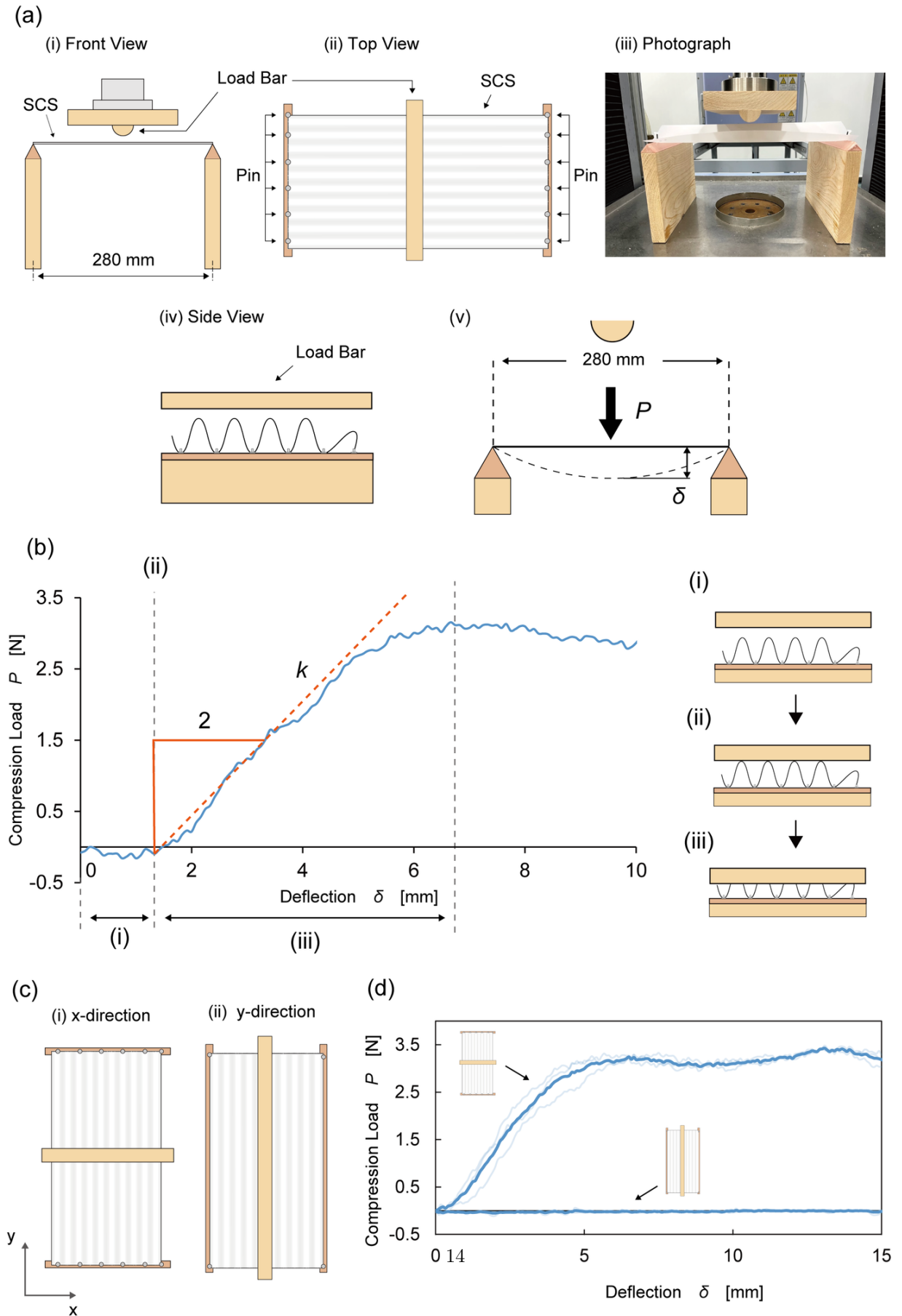


Figure 5: Stiffness evaluation of the SCS. a) Schematic of the three-point bending test; i) front view; ii) top view; iii) photograph; iv) side view; v) relationship between the load  $P$  and deflection  $\delta$ . b) Load-deflection curve obtained by three point bending test; i) before contact; ii) start of the test; iii) loaded. c) Confirmation

Rich media available at [https://youtu.be/\\_3phQd0zrmk](https://youtu.be/_3phQd0zrmk)

## Results and Discussion

We investigated the influence of the design parameters, linewidth  $L$ , and number of lines  $n$  on the stiffness of the SCS. The second area moment of the corrugated structure is expressed by the following equation [36]:

$$I = \frac{d^2 h}{2} \left[ 1 - \frac{0.81}{1 + 2.5 \left( \frac{d}{2w} \right)^2} \right] \quad (12)$$

Equation (12) expresses that with an increase in the amplitude of the corrugated structure, the second area moment increases. Thereafter, we derived the equation for the relationship between the second area moment and design parameters. By substituting Equation (7) and (8) into Equation (12), the relationship between the second area moment and design parameters is expressed by the following equation.

$$I = \frac{\left( 105 \cos\left(90 - \frac{mL}{2}\right) \right)^2 h}{2n^2} \left[ 1 - \frac{0.81}{1 + 2.5 \left( \frac{105 \cos\left(90 - \frac{mL}{2}\right)}{2 \times 210 \sin\left(90 - \frac{mL}{2}\right)} \right)^2} \right] \quad (13)$$

Equation (13) expresses that with a decrease in the number of lines and increase in the linewidth, the second area moment increases. **Figure 10a** presents the load-deflection curve obtained from the SCS fabricated with  $n = 4$  and 10 and the second area moment derived from the results. The SCS results fabricated with  $n = 6$  and 8 are presented in Supporting information (**Figure S2**). The translucent lines in the graph indicate the results of the three measurements, and the opaque lines indicate the averaged results. First, we evaluated the stiffness of the SCS fabricated with  $n = 10$  (Figure 10a(i)). The upper left of the photographs presents the SCS for  $n = 10$  with  $L = 5$  mm, 10 mm, and 15 mm. From the load-deflection curve, with an increase in the linewidth, the slope of the initial stage increased, and the stiffness increased. As a result, the second area moment increased. Therefore, as expressed as Equation (12) and (13), with an increase in the linewidth and amplitude of the SCS for  $n = 10$ , the stiffness of the structure with a higher second area moment increased. Moreover, as can be seen from the load-deflection curve at  $L = 15$  mm, the first peak load was 3.24 N, thus indicating that the structure can withstand a load of approximately 330 g. This indicates that a sheet of paper with a mass of 5.72 g can withstand a load greater than its mass by a factor of 57.7, thus acting as a SCS. The microstructure mentioned by Bassik et al. can withstand a load greater than its mass by 7700; however, it has the maximum load capacity of 0.883 g because the structure is small [7]. Using the proposed paper-printing self-folding technology, we successfully tailor-made a large-scale corrugated structure with various stiffness properties and high load capacity. Thereafter, we evaluated the stiffness of the structure with  $n = 4$  (Figure 10a(ii)). For the structure with  $n = 4$ , there was no increase in the slope of the initial stage with an increase in the linewidth, and the stiffness results exhibited a different trend from that expressed by Equation (12). Furthermore, despite the decrease in the number of lines, the second area moment was lower than  $n = 10$ , which exhibited a different trend from that expressed by Equation (13). In addition, although the SCS was fabricated with the same linewidth, there was a significant variation between the three tests. We found that the structural characteristics can be typical for self-folded corrugated structures such as the SCS.

Figure 10b presents the stiffness distribution of the fabricated SCS. Due to the reaction between the paper and printed solution, the stiffness of the crease parts increased in the SCS. However, the stiffness of the straight-line parts connecting the creases remained low because no new components were added, and no hard compression was used to process it. Therefore, with a decrease in the number of lines, there were more

straight-line parts with low stiffness; thus, there was a higher probability of deformation during the three-point bending test. Figure 10c presents the structure with  $n = 4$  and 10 immediately after the end of the three-point bending test. Compared with the structure with  $n = 10$ , the structure with  $n = 4$  underwent with significant deformation. Therefore, we considered that the increase in stiffness with an increase in amplitude could not be confirmed for the structure with  $n = 4$ . Thus, increasing the linewidth and amplitude is not sufficient to design an SCS with high stiffness; considering that the stiffness distribution over the entire SCS is required.

Furthermore, the results revealed that the load repeatedly increased or decreased in all the load-deflection curves. The results may indicate that the SCS buckle repeatedly during the three-point bending test. First, at the peak of the load, the mountain folds buckled, and the load decreased. After the buckling of the mountain folds, the residual part of the SCS received additional compressive load, which caused the buckling and increase or decrease of the load. This process was repeated during the test, thus causing the load to increase or decrease repeatedly. We attributed this to the flexibility of the paper material.

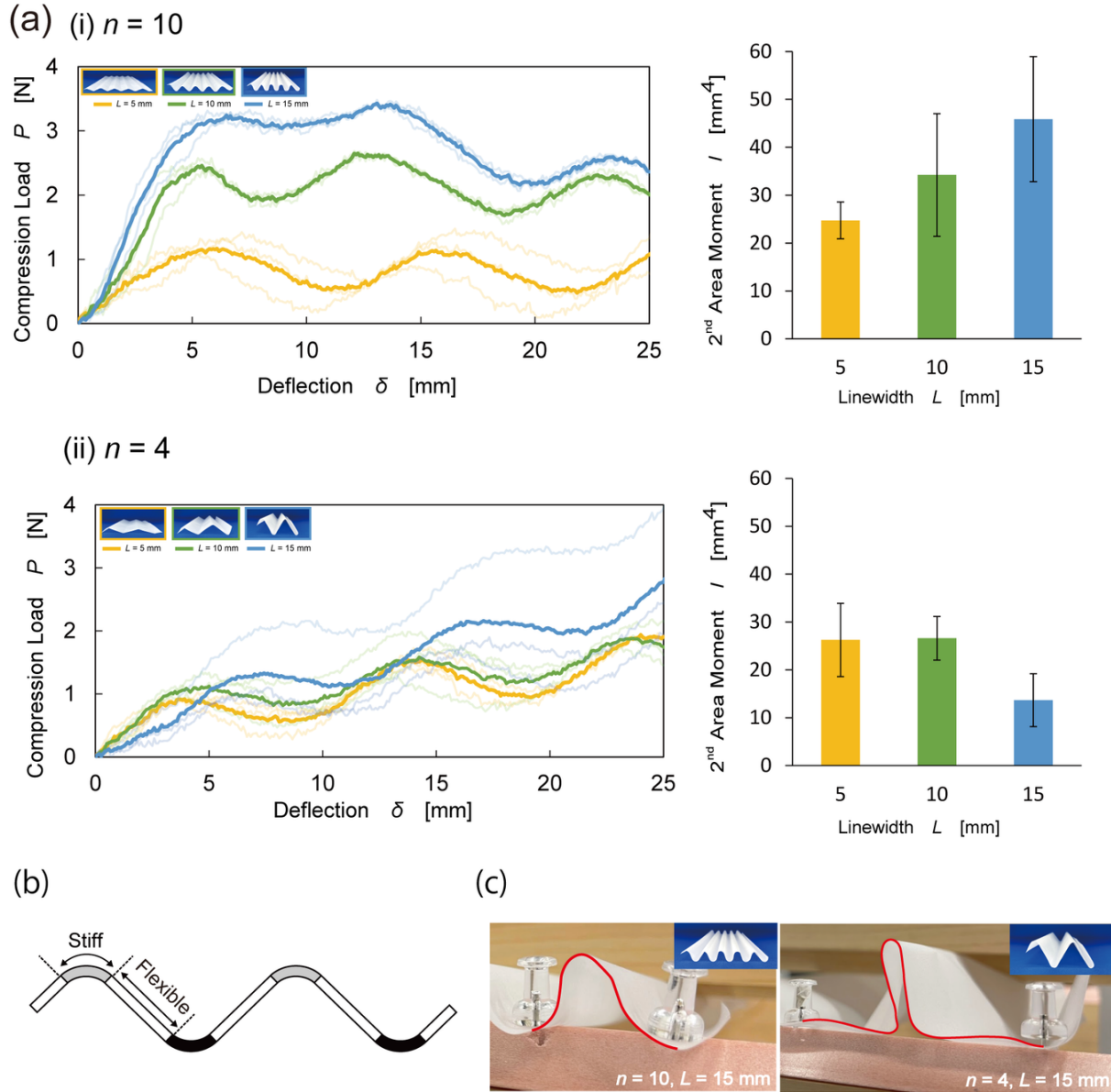


Figure 6: Stiffness evaluation of the SCS with respect to the linewidth  $L$  and number of lines  $n$ . Results of three-point bending tests with a) i)  $n = 10$  and ii)  $n = 4$ . Error bars indicate  $\pm 1$  SD. b) Stiffness distribution of the SCS. The crease parts where the ink was printed exhibited high stiffness, whereas the straight-line parts exhibited low stiffness. c) The SCS cross-section immediately after the completion of the three-point bending test. The SCS fabricated with  $n = 4$  was significantly deformed.

## Comparison with CAD Software and Stacking Performance

We designed equivalent corrugated models using CAD software (SolidWorks) and derived the second area moment. The values obtained from the experiment and CAD software were compared using SCSs fabricated with  $n = 10$  (Figure 11a). We created the SCS models using the measured amplitude  $d$  and half-

wavelength  $w$ , as shown in Figure 6d and the equation shown in Figure 11a. Figure 11b presents the results of the comparison. The simulation results were consistent with the experimental results, and the second area moment increased with an increase in amplitude. However, there were significant differences in the values. Furthermore, the amplitude dependence of the SCS stiffness exhibited a linear scaling relationship, which is different from the quadratic scaling expressed by Equation (12) and previous studies [31]. This is one of the characteristics of SCSs fabricated from flexible sheet materials and may be because the structure has not been deformed with maintaining the corrugated cross section. Figure 11c presents the mountain fold parts after the three-point bending test. The deformation of the mountain fold parts can be observed.

Due to the flexibility of the developed SCS, we found that the SCS can be stacked and strengthened without occupying space. Stacking a large number of sheets allows for the realization of the same strength as that of a sheet of thickness that would not inherently undergo self-folding. We fabricated 2, 3, and 10 sheets of the SCS with  $n = 10$  and linewidth  $L = 15$  mm. **Figure S3** presents the comparison between a one-sheet SCS and a 10-sheet SCS. Given that the SCS is thin and flexible, 10 sheets could be stacked without occupying a significant amount of space. We conducted a three-point bending test on the 2, 3, and 10 sheets of the stacked SCSs. Figure 11d and e present the results. As shown in Figure 11d (load-deflection curves), the slope of the initial stage increased, and the stiffness increased as the number of sheets stacks increased. Furthermore, the second area moment increased linearly with the number of sheets (181% for 1–2 sheets, 452% for 3 sheets, and 1461% for 10 sheets), as shown in Figure 11e. Hence, the stiffness of an SCS is dependent on the design parameters of the corrugated structures and the number of stacked sheets. Moreover, the load-deflection curve for 10-sheet stacking did not increase or decrease the load, as shown in Figure 11d. Based on this result, we inferred that only the mountain-folded part of the sheet buckled when 10 sheets were stacked, and the residual part of the SCS does not buckle. This can be attributed to the improvement of material strength by stacking 10 sheets.

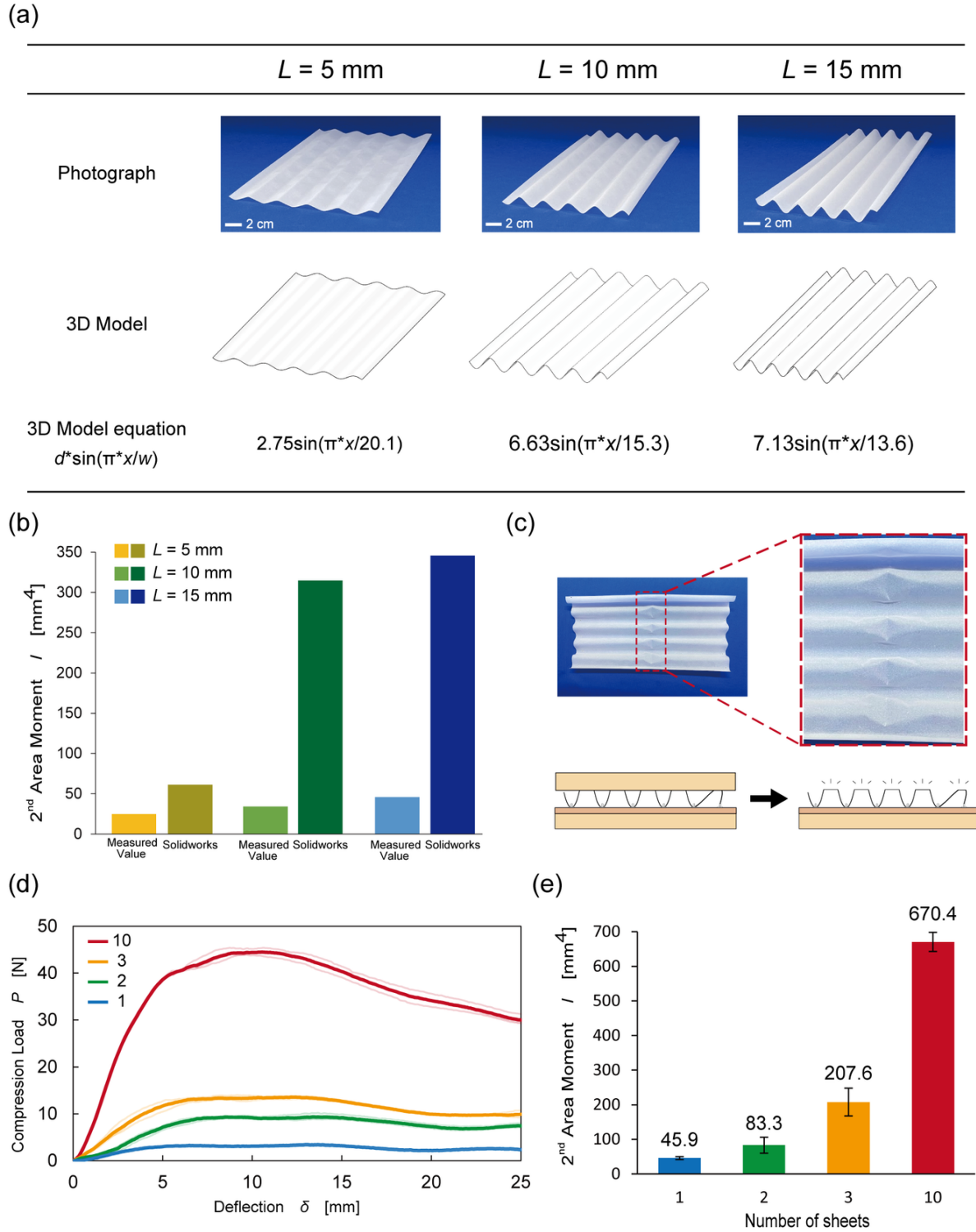


Figure 7: a) Comparison between the photograph and the 3D model when  $n = 10$  and  $L = 5, 10, 15 \text{ mm}$ . b) Comparison of the second area moment derived from the simulation and obtained from the experiment. c) Mountain fold parts of the SCS after the three-point bending test. Deformation occurred at the crease parts, and uniform deformation of the cross-sectional structure did not occur. d) Three-point bending test results of the stacked SCS (1, 2, 3, and 10 sheets) and e) the calculated second area moment. As stacking increased, the slope of the initial stage increased, and the second area moment increased linearly. The error bars indicate  $\pm 1 \text{ SD}$ .

## Conclusion

In this study, we developed an SCS that self-folds into high-strength structures from a single sheet of paper by inkjet printing. The concept of the SCS is based on the properties of the origami technique for enhancing structural strength. The SCS has the following design parameters: printing line width  $L$  and number of printing lines  $n$ . By changing these parameters, we fabricated an SCS with various amplitudes  $d$  and half-wavelengths  $w$ . Specifically, with an increase in the linewidth, the amplitude increased, and the half-wavelength decreased. Additionally, with an increase in the number of lines, the amplitude decreased, and half-wavelength changed with respect to  $L$ . This relationship was validated by measuring  $d$  and  $w$  for a total of 60 SCSs. Furthermore, by approximating the SCS cross-section as a triangle, we derived a linear approximation relationship between  $L$  and the fold angle  $\vartheta$ . The  $R^2$  values of the derived approximations were all close to one, which were consistent with the linear relationship between  $L$  and  $\vartheta$ . Based on this approximation, we derived a model for  $d$  and  $w$  of the SCS, which allowed for the design of an SCS with the desired shape. Thereafter, we developed a methodology to design the SCS of the desired shape by self-folding a paper.

Furthermore, we conducted 36 three-point bending tests on 12 types of SCSs with different design parameters to evaluate their mechanical properties. By evaluating the mechanical properties, we established the design theory of an SCS with high stiffness. Corrugated structures have higher second area moments at higher amplitudes [36]. However, the three-point bending test results revealed that the SCS with the highest amplitude deformed significantly under loading, and the second area moment decreased. This is because the SCS exhibited a non-uniform stiffness of printed and unprinted parts in its self-folded structure. To fabricate an SCS with higher strength, it is not sufficient to simply design a higher amplitude. In particular, it is necessary to consider the stiffness distribution throughout the SCS. Moreover, we evaluated the mechanical property of the SCS stacked with 2, 3, and 10 sheets to verify the strength-enhancing effect of the stacking sheets. As observed, the second area moment of 10 sheets was 1461% higher than that of one sheet.

The proposed SCS could be designed and fabricated rapidly to achieve the desired shape and stiffness. As the material is paper, the SCS is inexpensive and recyclable. Additionally, the flexibility of the paper material allows for it to be stacked without occupying a significant amount of space, even after forming the SCS. Moreover, it improves the stiffness without requiring additional components. Hence, the proposed SCS is a promising smart core material that self-folds while maintaining the stiffness required by the core material of the sandwich structure. Moreover, it does not create space before or after self-folding, and demonstrates a high transport performance. Based on the stiffness investigation, it was confirmed that the SCS exhibits anisotropic stiffness. Hence, the SCS can be used in applications that require load-bearing, such as the core material of sandwich structures; in addition to anisotropy, e.g., as morphing wings and the skeleton of pneumatic actuators [37]. More complex and robust structures can be created by filling the printer with various chemicals and ordering the folding sequence [33]. By printing electrodes on the same paper surface, the application of intelligent core materials with integrated actuators and sensors can be realized in the future [34].

## Supporting Information

The supporting information file related to our article is hosted on Authorea.

## Conflict of Interest

The authors declare no conflict of interest.

## Acknowledgements

This work was supported by JSPS KAKENHI, grant numbers 18H05895 and 19K20377. This research is supported by Adaptable and Seamless Technology transfer Program through Target-driven R&D (A-STEP) from Japan Science and Technology Agency (JST) Grant Number JPMJTM20CK. This research is supported by SIT International Research Center for Green Electronics. We would like to thank Editage ([www.editage.com](http://www.editage.com)) for English language editing.

## References

- [1] K. Kuribayashi *et al.*, “Self-deployable origami stent grafts as a biomedical application of Ni-rich TiNi shape memory alloy foil”, *Materials Science and Engineering: A*, vol. 419, no. 1-2, pp. 131–137, 2006.
- [2] J. T. Bruton, T. G. Nelson, T. K. Zimmerman, J. D. Fernelius, S. P. Magleby, and L. L. Howell, “Packing and deploying Soft Origami to and from cylindrical volumes with application to automotive airbags”, *Royal Society open science*, vol. 3, no. 9, p. 160429, 2016.
- [3] A. P. Thrall and C. P. Quaglia, “Accordion shelters: A historical review of origami-like deployable shelters developed by the US military”, *Engineering structures*, vol. 59, pp. 686–692, 2014.
- [4] S. A. Zirbel *et al.*, “Accommodating thickness in origami-based deployable arrays”, *Journal of Mechanical Design*, vol. 135, no. 11, 2013.
- [5] S. R. Woodruff and E. T. Filipov, “Curved creases redistribute global bending stiffness in corrugations: theory and experimentation”, *Meccanica*, vol. 56, no. 6, pp. 1613–1634, 2021.
- [6] W. Gilewski, J. Pelczyński, and P. Stawarz, “A comparative study of Origami inspired folded plates”, *Procedia Engineering*, vol. 91, pp. 220–225, 2014.
- [7] N. Bassik, G. M. Stern, and D. H. Gracias, “Microassembly based on hands free origami with bidirectional curvature”, *Applied physics letters*, vol. 95, no. 9, p. 091901, 2009.
- [8] W. He, L. Yao, X. Meng, G. Sun, D. Xie, and J. Liu, “Effect of structural parameters on low-velocity impact behavior of aluminum honeycomb sandwich structures with CFRP face sheets”, *Thin-Walled Structures*, vol. 137, pp. 411–432, 2019.
- [9] K. Saito, S. Pellegrino, and T. Nojima, “Manufacture of arbitrary cross-section composite honeycomb cores based on origami techniques”, *Journal of Mechanical Design*, vol. 136, no. 5, p. 051011, 2014.
- [10] K. Miura and R. J. Lang, “The science of Miura-ori: A review”, *Origami*, vol. 4, pp. 87–99, 2009.
- [11] R. D. Resch, “Self-supporting structural unit having a series of repetitious geometrical modules”. Google Patents, Oct-1968.
- [12] C. Zhou, Z. Wang, and P. Weaver, “Thermal-mechanical optimization of V-pattern folded core sandwich panels for thermal protection systems”, in *2017 8th International Conference on Mechanical and Aerospace Engineering (ICMAE)*, 2017, pp. 354–359.
- [13] T. Yokozeki, S.-ichi Takeda, T. Ogasawara, and T. Ishikawa, “Mechanical properties of corrugated composites for candidate materials of flexible wing structures”, *Composites Part A: applied science and manufacturing*, vol. 37, no. 10, pp. 1578–1586, 2006.

- [14]I. Dayyani, A. D. Shaw, E. I. S. Flores, and M. I. Friswell, “The mechanics of composite corrugated structures: A review with applications in morphing aircraft”, *Composite Structures*, vol. 133, pp. 358–380, 2015.
- [15]H. A. Katzman, R. M. Castaneda, and H. S. Lee, “Moisture diffusion in composite sandwich structures”, *Composites Part A: Applied Science and Manufacturing*, vol. 39, no. 5, pp. 887–892, 2008.
- [16]D. J. Balkcom and M. T. Mason, “Robotic origami folding”, *The International Journal of Robotics Research*, vol. 27, no. 5, pp. 613–627, 2008.
- [17]E. A. Peraza-Hernandez, D. J. Hartl, R. J. Malak Jr, and D. C. Lagoudas, “Origami-inspired active structures: a synthesis and review”, *Smart Materials and Structures*, vol. 23, no. 9, p. 094001, 2014.
- [18]E. A. Peraza-Hernandez, D. J. Hartl, and R. J. Malak Jr, “Design and numerical analysis of an SMA mesh-based self-folding sheet”, *Smart Materials and Structures*, vol. 22, no. 9, p. 094008, 2013.
- [19]Q. Ge, A. H. Sakhaei, H. Lee, C. K. Dunn, N. X. Fang, and M. L. Dunn, “Multimaterial 4D printing with tailorable shape memory polymers. *Sci Rep* 6: 31110”. 2016.
- [20]N. An, M. Li, and J. Zhou, “Predicting origami-inspired programmable self-folding of hydrogel trilayers”, *Smart Materials and Structures*, vol. 25, no. 11, p. 11LT02, 2016.
- [21]Y. Liu, J. K. Boyles, J. Genzer, and M. D. Dickey, “Self-folding of polymer sheets using local light absorption”, *Soft matter*, vol. 8, no. 6, pp. 1764–1769, 2012.
- [22]M. R. M. Rejab and W. J. Cantwell, “The mechanical behaviour of corrugated-core sandwich panels”, *Composites Part B: Engineering*, vol. 47, pp. 267–277, 2013.
- [23]B. Du *et al.*, “Fabrication and bending behavior of thermoplastic composite curved corrugated sandwich beam with interface enhancement”, *International Journal of Mechanical Sciences*, vol. 149, pp. 101–111, 2018.
- [24]S. Heimbs, “Foldcore sandwich structures and their impact behaviour: an overview”, *Dynamic failure of composite and sandwich structures*, pp. 491–544, 2013.
- [25]T. Li and L. Wang, “Bending behavior of sandwich composite structures with tunable 3D-printed core materials”, *Composite Structures*, vol. 175, pp. 46–57, 2017.
- [26]G. D. Goh, S. J. C. Neo, V. Dikshit, and W. Y. Yeong, “Quasi-static indentation and sound-absorbing properties of 3D printed sandwich core panels”, *Journal of Sandwich Structures & Materials*, p. 10996362211037015, 2021.
- [27]L. Meng, X. Qiu, T. Gao, Z. Li, and W. Zhang, “An inverse approach to the accurate modelling of 3D-printed sandwich panels with lattice core using beams of variable cross-section”, *Composite Structures*, vol. 247, p. 112363, 2020.
- [28]Y. Feng, H. Qiu, Y. Gao, H. Zheng, and J. Tan, “Creative design for sandwich structures: A review”, *International Journal of Advanced Robotic Systems*, vol. 17, no. 3, p. 1729881420921327, 2020.
- [29]M. T. Tolley, S. M. Felton, S. Miyashita, D. Aukes, D. Rus, and R. J. Wood, “Self-folding origami: shape memory composites activated by uniform heating”, *Smart Materials and Structures*, vol. 23, no. 9, p. 094006, 2014.
- [30]J.-H. Na *et al.*, “Programming reversibly self-folding origami with micropatterned photo-crosslinkable polymer trilayers”, *Advanced Materials*, vol. 27, no. 1, pp. 79–85, 2015.
- [31]A. M. Hubbard, J. K. Patel, S. Wagner, C.-H. Chang, J. Genzer, and M. D. Dickey, “Stiff or Extensible in Seconds: Light-Induced Corrugations in Thin Polymer Sheets”, *Advanced Materials Technologies*, vol. 6, no. 1, p. 2000789, 2021.

- [32]H. Shigemune, S. Maeda, Y. Hara, N. Hosoya, and S. Hashimoto, “Origami robot: a self-folding paper robot with an electrothermal actuator created by printing”, *IEEE/ASME Transactions On Mechatronics*, vol. 21, no. 6, pp. 2746–2754, 2016.
- [33]H. Shigemune, S. Maeda, E. Iwase, S. Hashimoto, S. Sugano, and H. Sawada, “Programming Stepwise Motility into a Sheet of Paper Using Inkjet Printing”, *Advanced Intelligent Systems*, vol. 3, no. 1, p. 2000153, 2021.
- [34]H. Shigemune *et al.*, “Printed paper robot driven by electrostatic actuator”, *IEEE Robotics and Automation Letters*, vol. 2, no. 2, pp. 1001–1007, 2017.
- [35]Y. Liu, J. Genzer, and M. D. Dickey, “‘2D or not 2D’: Shape-programming polymer sheets”, *Progress in Polymer Science*, vol. 52, pp. 79–106, 2016.
- [36]S. Timoshenko and S. Woinowsky-Krieger, “Theory of plates and shells”, 1959.
- [37]S. Li, D. M. Vogt, D. Rus, and R. J. Wood, “Fluid-driven origami-inspired artificial muscles”, *Proceedings of the National academy of Sciences*, vol. 114, no. 50, pp. 13132–13137, 2017.